ROYAL SOCIETY
OF CHEMISTRY

## PAPER

Check for updates

# Interfacial passivation with 4-chlorobenzene sulfonyl chloride for stable and efficient planar perovskite solar cells†

Foo Shini,‡[abc] M. Thambidurai, [ID] ‡[ab] Herlina Arianita Dewi,[b] Nur Fadilah Jamaludin,[b] Annalisa Bruno, [ID] [b] Anil Kanwat, [ID] [b] Nripan Mathews, [ID] [bc] Cuong Dang [ID] *[ab] and Hung D. Nguyen*[ab]

The interfacial passivation technique is an effective method to improve the stability and photovoltaic performance of perovskite solar cells. Here, we demonstrate the importance of passivating undercoordinated halide ions in minimizing carrier losses at the perovskite/spiro-OMeTAD interface. 4-Chlorobenzene sulfonyl chloride (CBSC) has been utilized as a Lewis acid passivation material. CBSC molecules act as electron acceptors, which bind to the negatively charged undercoordinated halide ions and Pb−I antisite defects ($PbI_3^-$). The champion CBSC-passivated perovskite device shows a high power conversion efficiency (PCE) of 20.02%, unlike the pristine device with an efficiency of 18.29%. Significant long term-stability in the CBSC passivated device is also observed, maintaining 93% of the initial PCE after 768 h stored in ambient conditions with 30% relative humidity.

## 1. Introduction

Organic–inorganic perovskite solar cells (PSCs) have attracted significant attention due to their low-cost and high-power conversion efficiency (PCE) achieved to date.[1–5] Despite this, the maximum PCE of current state-of-the-art PSCs ($>25\%$) remains far below the Shockley–Quisser limit of over 30%, assuming no other losses apart from radiative recombination of solar cells.[6–8] Therefore, it is critical that defects (bulk and interfacial) – primary contributors to non-radiative recombination losses – be effectively managed to improve device efficiency. While bulk defects can be mitigated with compositional or additive engineering, it is noted that major losses in PSCs arise from surface defects, especially at the interfaces between the perovskite absorber and adjacent charge selective transport layers.[9–11] Despite the facile fabrication of compact and uniform perovskite films *via* solution-based processing, the tendency for surface

defect formation – a result of rapid crystallization and post-deposition annealing – is high. These defects, including pinholes, grain boundaries, under-coordinated ions, dangling bonds, and non-stoichiometric composition on the surface, could lead to non-radiative charge recombination, which can severely hamper the photovoltaic performance of PSCs and may simultaneously induce perovskite degradation.[12–16]

One of the more direct and efficient strategies of managing perovskite surface defects and ensuring efficient charge transport into the adjacent interlayers is through interface passivation.[17–20] Several works on interfacial passivation in PSCs have been reported previously. For example, post-treatment on the perovskite surface using a two-dimensional (2D) perovskite, polymer, or organic ammonium salt, as well as inducing Lewis acid or base reactions, have shown the capability of improving both the PSC efficiency and stability.[21–26] The mitigation of surface defects translates to an increase in open circuit voltage ($V_{oc}$) arising from enhanced charge extraction. Liu and coworkers applied 2-aminoterephthalic acid as the passivation layer between the perovskite and Spiro-OMeTAD, leading to improved hydrophobicity of the perovskite film and PCE of 21.09%.[27] Yi and coworkers utilized phenylhydroxylammonium halide (PBABr) salts to passivate the perovskite surface, and it was found that PBABr treatment can reduce the trap density and give a longer carrier lifetime.[28] Recently, Huang *et al.*, reported that 4-chlorobenzene sulfonyl chloride (CBSC) as a hydro-stable self-assembled small-molecule was utilized in organic solar cells, which enhanced the surface energy, gave a higher absorption coefficient, and tuned the work

[a] *Centre for OptoElectronics and Biophotonics (COEB), School of Electrical and Electronic Engineering, The Photonics Institute (TPI), Nanyang Technological University, 50 Nanyang Avenue, 639798, Singapore. E-mail: hcdang@ntu.edu.sg, hunghtd@ntu.edu.sg*

[b] *Energy Research Institute @NTU (ERI@N), Research Techno Plaza, X-Frontier Block, Level 5, 50 Nanyang Drive, 637553, Singapore*

[c] *School of Materials Science and Engineering, Nanyang Technological University, 50 Nanyang Avenue, 639798, Singapore*

† Electronic supplementary information (ESI) available. See DOI: **https://doi.org/10.1039/d2tc00982j**

‡ Foo Shini and M. Thambidurai contributed equally.

function, resulting in a PCE of 10.6%.[29] Hence, CBSC passivation materials could be expected to improve the PCE and stability of perovskite devices. Nevertheless, it is still challenging to determine the several effects of suitable morphology, surface defect passivation, hydrophobicity, and optoelectronic properties to further boost the PCE and stability of perovskite devices. Here, spin coating of a thin CBSC ($ClC_6H_4SO_2Cl$) layer on the $Cs_{0.05}(MA_{0.17}FA_{0.83})_{0.95}Pb(I_{0.83}Br_{0.17})_3$ perovskite film yielded enhanced PCEs. The PCE of the CBSC passivated device was 20.02%, versus 18.29% in the control device. The CBSC-passivated PSCs show a $\sim 50$ mV increase in $V_{oc}$ as compared to the pristine sample, confirming successful surface defect passivation. The champion CBSC-passivated PSC exhibited an efficiency of 20.02% with a high PCE retention of $\sim 93\%$ when stored under a controlled environment (relative humidity of 30% and room temperature) for 768 hours.

## 2. Results and discussion

X-Ray diffraction (XRD) measurement was used to investigate the pristine and different concentrations (3, 5, and 7 mg mL$^{-1}$) of CBSC-passivated perovskite films. As seen in Fig. 1a, the films exhibit similar diffraction patterns corresponding to a tetragonal crystal structure despite the various CBSC concentrations employed. Furthermore, all samples display a characteristic $PbI_2$ peak at 12.5° due to the presence of excess $PbI_2$ in the perovskite precursor solution.[30–33] As depicted in Fig. 1a, the full width at half maximum (FWHM) decreases from 0.428 for pristine perovskite to 0.340, 0.310, and 0.329 for the 3, 5 and 7 mg mL$^{-1}$ CBSC passivated perovskite film. The smaller FWHM represents good crystallinity of the perovskite. A field emission scanning electron microscope (FESEM) was used to study the effect of the CBSC passivation layer on the film

morphologies, as displayed in Fig. 1b–e. Both pristine and passivated films exhibit dense, uniform, and smooth surface morphologies. That being said, CBSC passivated films exhibit slightly larger grain sizes when compared to the pristine perovskite film. The average grain sizes of the 0 mg mL$^{-1}$ (prisitine), 3 mg mL$^{-1}$, 5 mg mL$^{-1}$ and 7 mg mL$^{-1}$ CBSC passivated films are 220, 280, 310 and 290 nm, respectively.

To understand the effects of CBSC passivation on the perovskite films, UV-vis spectroscopy was employed. Specifically, perovskite films were treated with CBSC of concentrations up to 7 mg mL$^{-1}$ prior to testing. As seen in Fig. 2a, the absorption spectra of CBSC treated perovskite films exhibit a redshift when compared to that of the pristine film. As presented in Fig. S1, (ESI†) the band gaps of pristine and 5 mg mL$^{-1}$ CBSC treated perovskite were estimated to be 1.63 eV and 1.62 eV, respectively, indicating a little improvement of light absorption after CBSC passivation. Fig. 2b presents the steady-state photoluminescence (PL) spectra of the pristine and CBSC-passivated perovskite films. It is evident that the addition of CBSC, regardless of concentration, provides effective passivation of defects. All the CBSC-passivated films showed increased PL intensities with the highest observed in the 5 mg mL$^{-1}$ CBSC passivated film while retaining a similar PL emission profile (757 nm). The drop of PL intensity for the 7 mg mL$^{-1}$ CBSC-passivated perovskite films suggests that the employment of CBSC concentration beyond 5 mg mL$^{-1}$ is detrimental to the film's optical properties. Moreover, utilization of excessive passivation material has previously been shown to induce more trap states at the perovskite/ HTL interface.[34–37] Henceforth, it is essential that an optimal concentration of passivation material is employed to yield the desired defect passivation effect.

The time-resolved photoluminescence (TRPL) measurements were characterized to further analyze charge carrier dynamics and defect states of pristine and CBSC passivated perovskite
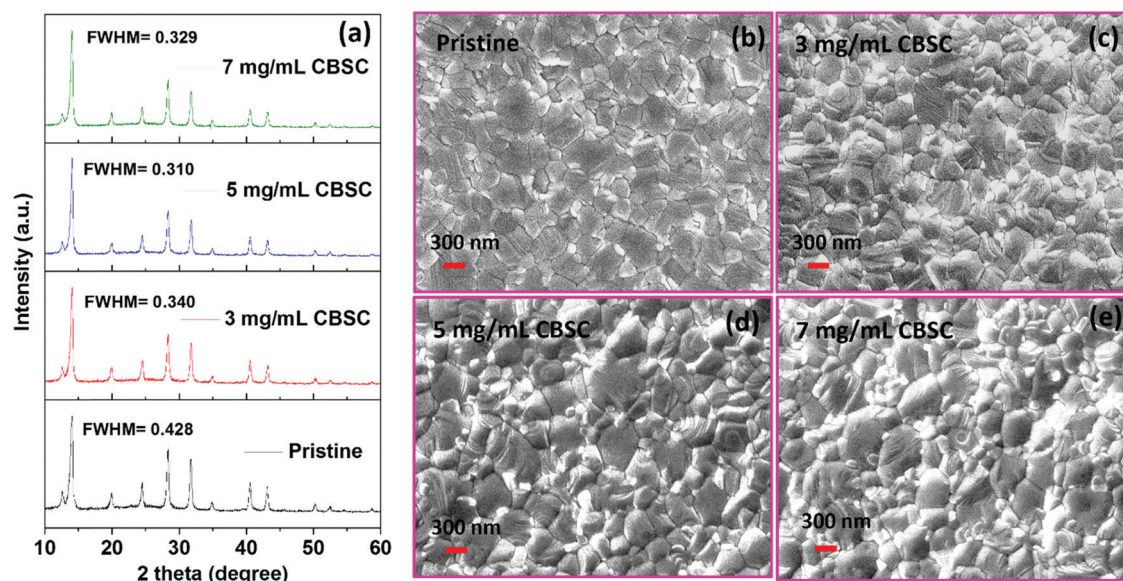


Fig. 1 (a) XRD patterns and (b–e) SEM images of pristine and CBSC passivated perovskite films.
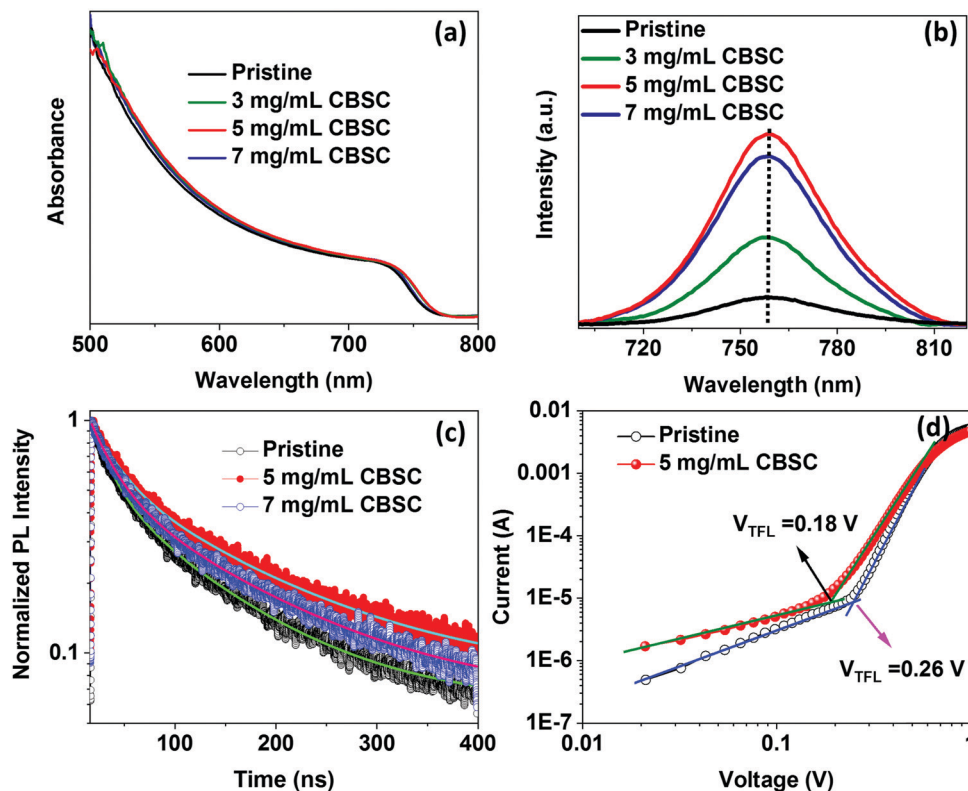
**Fig. 2** (a) Absorbance, (b) photoluminescence, and (c) TRPL spectra of pristine and CBSC passivated perovskite films. (d) Dark current−voltage (*I−V*) curves of electron only devices.

films, as depicted in Fig. 2c. The TRPL decay curves are fitted by a bi-exponential function and the corresponding fitted data are

displayed in Table S1 (ESI†). The average carrier lifetime of pristine, 5 mg mL$^{-1}$, and 7 mg mL$^{-1}$ CBSC passivated perovskite
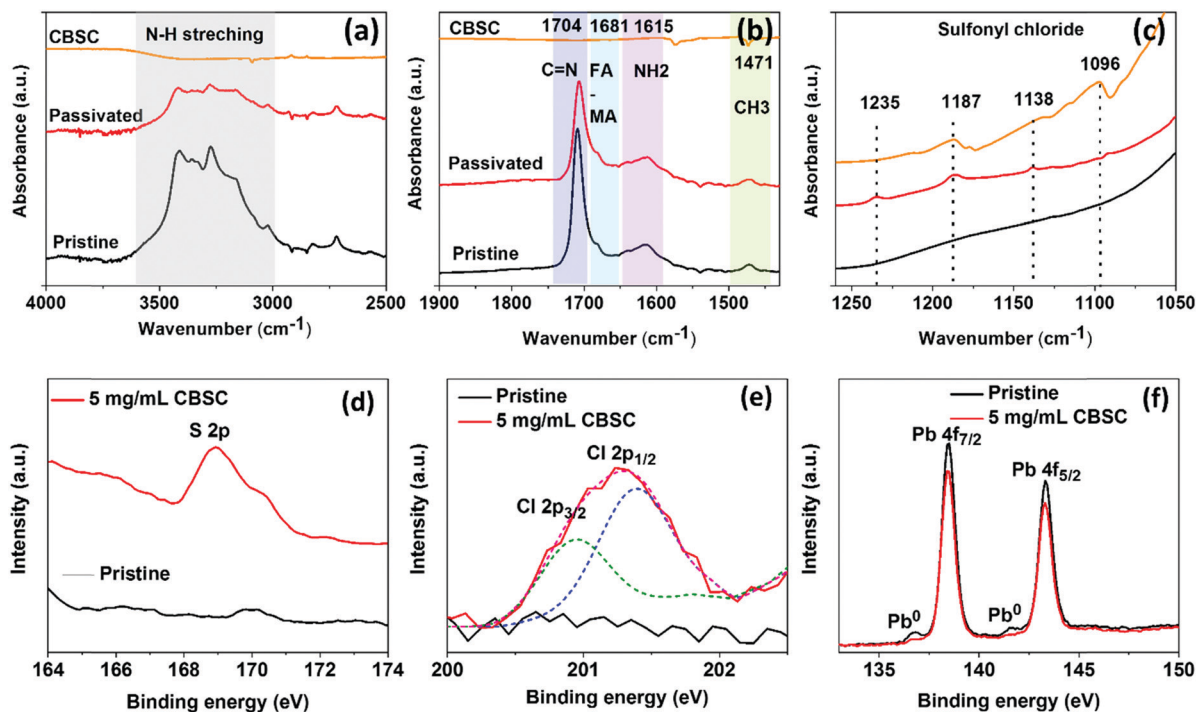


**Fig. 3** (a−c) ATR-FTIR spectra of pristine, CBSC passivated and pristine CBSC films. XPS spectra of the pristine and 5 mg mL$^{-1}$ CBSC passivated films, specifically (d) S 2p, (e) deconvoluted Cl 2p, and (f) Pb 4f.

**9046** | *J. Mater. Chem. C*, 2022, **10**, 9044–9051

This journal is © The Royal Society of Chemistry 2022

films are 48.40, 72.42 and 61.73 ns, respectively. Both PL and TRPL results indicate reduced surface defects and improved PCE in the CBSC passivated film. To investigate defect state densities of pristine and passivated perovskite film, space charge-limited current (SCLC) measurement was performed. Depicted in Fig. 2d are the dark current–voltage (I–V) characteristics of the electron only device with a structure of FTO/TiO$_2$/SnO$_2$/perovskite with or without CBSC/PCBM/Ag. The trap density ($N_{trap}$) of the pristine perovskite without and with a CBSC passivation device was determined using the equation $N_{trap} = 2\varepsilon\varepsilon_0 V_{TFL}/eL^2$, where $\varepsilon,\varepsilon_0$, $V_{TFL}$, $e$ and $L$ represent the relative dielectric constant of the perovskite, vacuum permittivity, trap filled limit voltage, elemental charge, and film thickness of the perovskite, respectively.[38] The trap filled limit voltage ($V_{TFL}$) values were obtained to be 0.26 V and 0.18 V for pristine and CBSC based devices, respectively, and the corresponding $N_{trap}$ values were estimated to be $2.66 \times 10^{15}$ cm$^{-3}$ and $1.84 \times 10^{15}$ cm$^{-3}$, respectively.

In order to disclose the CBSC molecular interaction in the mixed cation perovskite, we perform attenuated reflectance Fourier transform infrared spectroscopy (ATR-FTIR). The FTIR

spectra of the as-prepared pristine perovskite film, CBSC passivated film, and CBSC powder were obtained as shown in Fig. 3(a–c). The characteristic peaks depict N–H stretching at higher wavenumber, confirming the perovskite phase formation. The peaks at 1705, 1681, and 1615 cm$^{-1}$ are characteristic C=N stretching of the FA$^+$ cation, FA–MA complex, and NH$_2$ scissoring vibration, respectively.[39,40] The CBSC molecule in the passivated films is confirmed by the presence of sulfonyl chloride characteristic peaks found at lower wavenumber (1250–1050 cm$^{-1}$). We found slight displacement of the C=N stretching peaks in the CBSC passivated film, indicating possible interaction of the CBSC molecule with the perovskite.

To confirm the presence and effects of CBSC passivation, X-ray photoelectron spectroscopy (XPS) measurements were carried out on the as-prepared perovskite films. In Fig. 3d, the sulfur (S 2p) spectrum shows a peak at 168.95 eV. Fig. 3e shows the deconvoluted Cl characteristic peaks at 200.9 eV and 201.3 eV representing the Cl 2p$_{3/2}$ and 2p$_{1/2}$ peaks. Cheng and coworkers demonstrated a series of chlorobenzoic acids with varied positions and degrees of chlorination on the molecules and it was found that the binding energies of the Cl (organic molecule)
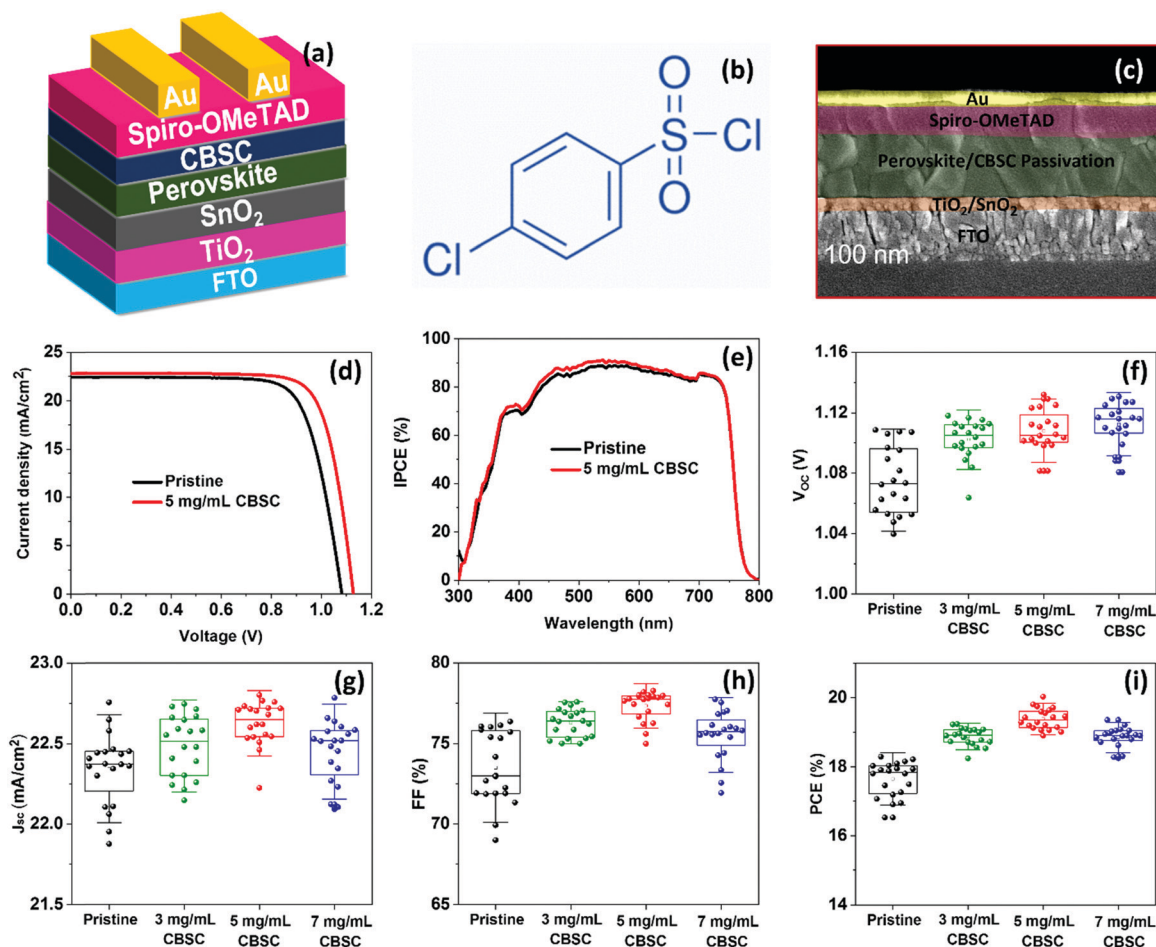


Fig. 4 (a) Device architecture of perovskite solar cells, (b) chemical structure of a CBSC molecule, and (c) cross-sectional SEM image of the CBSC passivated devices. (d) The J–V curve of the pristine and CBSC passivated devices. (e) IPCE spectra of the pristine and CBSC passivated devices. Statistical distribution of the photovoltaic parameters for all devices, specifically the (f) $V_{oc}$, (g) $J_{sc}$, (h) FF, and (i) PCE.

This journal is © The Royal Society of Chemistry 2022

J. Mater. Chem. C, 2022, **10**, 9044–9051 | **9047**

peaks at 201.2 and 202.8 eV were associated with Cl $2p_{3/2}$ and Cl $2p_{1/2}$, respectively. In addition, the chloride (Cl $2p_{3/2}$) binding energy is 198.9 eV, which is considered as Cl-ITO.[41] The presence of a Cl peak in the CBSC-passivated perovskite films, contrary to the pristine ones, strongly supports the successful addition of CBSC molecules. The highly electronegative chlorine atoms in the CBSC molecule inductively withdraw electron density from the sulfur (S) atom within the sulfonyl group $(R–S(=O)_2–R')$, leaving behind a partial positive charge on the sulfur atom. Hence, the sulfur atom acts as an electron acceptor to form coordination bonds with negatively charged defects such as Pb–I antisites ($PbI_3^-$) and/or undercoordinated $I^-$ ions.[42–44] Fig. 3f and Fig. S2 (ESI†) show the signals of the lead (Pb) 4f and iodine (I) 2p peaks, respectively. The Pb element is represented by two main peaks, namely, Pb $4f_{7/2}$ and Pb $4f_{5/2}$ at respective binding energies of 138.2 and 143.3 eV. On the other hand, the I element is represented by two main peaks, namely, I $3d_{5/2}$ and I $3d_{3/2}$ at respective binding energies of 619.2 and 630.6 eV. With the reduction in peak intensity for both the Pb and I spectra in the CBSC-passivated perovskite film, it is clear that the addition of CBSC molecules at the perovskite/spiro–OMeTAD does passivate the defects. It is interesting to note that while peaks at 136.8 and 141.5 eV corresponding to metallic $Pb^0$ are present in the pristine perovskite film, neither were observed on the addition of CBSC, further justifying its role as a passivator.[45,46]

Fig. 4a shows the complete CBSC-passivated PSC adopting a planar n–i–p structure device configuration consisting of FTO/c-TiO$_2$/SnO$_2$/perovskite/CBSC/spiro–OMeTAD/Au. The chemical structure of the CBSC molecule is shown in Fig. 4b. Although the chlorine (Cl) atoms found in the CBSC molecule have non-bonding valence electron pairs, the highly electronegative nature of the electron-withdrawing chlorine atoms far outweighs the donation of electron density from the lone pair. The cross-sectional SEM image of the PSC device is shown in Fig. 4c, with the thickness of the compact c-TiO$_2$/SnO$_2$, perovskite/CBSC, spiro-OMeTAD, and Au films noted to be 80, 520, 250, and 80 nm, respectively. To understand the effectiveness of the passivated perovskite devices for photovoltaic applications, current density against voltage ($J$–$V$) measurements tested at AM 1.5 G illumination (class AAA solar simulator, Newport Oriel Sol3A, 100 mW cm$^{-2}$) were conducted for the pristine and CBSC-passivated devices. Fig. 4d and Fig. S3 (ESI†) represent the $J$–$V$ curves of the pristine and CBSC-passivated devices collected under reverse scan. The highest PCE was achieved with the 5 mg mL$^{-1}$ CBSC-passivated device,

suggesting optimal passivator concentration for photovoltaic performance. As seen in Table 1, the nonpareil photovoltaic performance observed in the 5 mg mL$^{-1}$ CBSC device attained short-circuit current density ($J_{sc}$), open-circuit voltage ($V_{oc}$), fill factor (FF) and PCE of 22.80 mA cm$^{-2}$, 1.13 V, 77.79 and 20.02%, respectively. While lower concentrations of CBSC do not offer sufficient passivating effect, higher concentrations, on the other hand, are detrimental for device performance owing to the introduction of undesired trapped sites, resulting in lower $J_{sc}$ and FF values.[47,48] This is further supported by the PL trend mentioned previously (Fig. 2b). Given these points, the use of the optimal concentration of passivation material is of paramount importance for superior device performance to be achieved. In accordance with the results obtained from the $J$–$V$ measurements, the pristine device showed the poorest PCE of 18.29% with $J_{sc}$, $V_{oc}$ and FF of 22.43 mA cm$^{-2}$, 1.08 V and 75.4, respectively. Enhancement to $V_{oc}$ and FF suggests effective defect passivation provided by the CBSC molecules.[49] Fig. 4e is the incident photon-to-current conversion efficiency (IPCE) spectra of pristine and CBSC passivated devices. The integrated $J_{sc}$ value of the CBSC passivated device is 20.82 mA cm$^{-2}$, higher than that of the pristine device (20.43 mA cm$^{-2}$), and is in good agreement with the $J_{sc}$ value extracted from the $J$–$V$ curve. Fig. S4(a and b) (ESI†) presents the $J$–$V$ curves of the pristine and 5 mg mL$^{-1}$ CBSC passivated PSC devices when reverse and forward bias were applied. Unsurprisingly, a drop in hysteresis was noted when 5 mg mL$^{-1}$ of CBSC was deposited on top of the perovskite film (Table S2, ESI†). Based on the calculation of hysteresis index (HI) = $\dfrac{\text{PCE(reverse)} - \text{PCE(forward)}}{\text{PCE(reverse)}}$, HI for the 5 mg mL$^{-1}$ CBSC-passivated device is approximately 0.07 while that of the pristine device is 0.17.[50] The smaller degree of hysteresis noted for the 5 mg mL$^{-1}$ CBSC-passivated perovskite device could be attributed to the successful passivation of defects, which reduces the susceptibility of charge trapping and de-trapping phenomena thought to play a part in hysteresis behavior.[51] The steady-state photocurrent and PCE of the champion devices measured at the maximum power point tracking (MPPT) under AM 1.5 G illumination are displayed in Fig. S5(a and b). The CBSC passivated device shows a $J_{sc}$ of 20.69 mA cm$^{-2}$, and a PCE of 19.02% under an applied voltage bias of 0.92 V. On the other hand, the pristine device exhibits a $J_{sc}$ of 19.69 mA cm$^{-2}$, and a PCE of 17.38% under a voltage bias of 0.88 V.

To understand the trends and device reproducibility of the pristine and CBSC-passivated devices, 20 devices were prepared

**Table 1** Photovoltaic parameters of pristine and CBSC passivated perovskite solar cells

| Devices | Devices | $V_{oc}$ [V] | $J_{sc}$ [mA cm$^{-2}$] | FF [%] | PCE [%] |
|---|---|---|---|---|---|
| Pristine | Best | 1.08 | 22.43 | 75.40 | 18.29 |
| | Average | 1.07 ± 0.02 | 22.34 ± 0.22 | 73.49 ± 2.25 | 17.65 ± 0.50 |
| 3 mg mL$^{-1}$ CBSC | Best | 1.11 | 22.66 | 76.23 | 19.23 |
| | Average | 1.10 ± 0.01 | 22.48 ± 0.18 | 76.28 ± 0.86 | 18.88 ± 0.25 |
| 5 mg mL$^{-1}$ CBSC | Best | 1.13 | 22.80 | 77.79 | 20.02 |
| | Average | 1.10 ± 0.01 | 22.62 ± 0.13 | 77.33 ± 0.91 | 19.38 ± 0.30 |
| 7 mg mL$^{-1}$ CBSC | Best | 1.13 | 22.48 | 76.15 | 19.35 |
| | Average | 1.11 ± 0.01 | 22.44 ± 0.19 | 75.51 ± 1.54 | 18.85 ± 0.29 |

9048 | *J. Mater. Chem. C*, 2022, **10**, 9044–9051
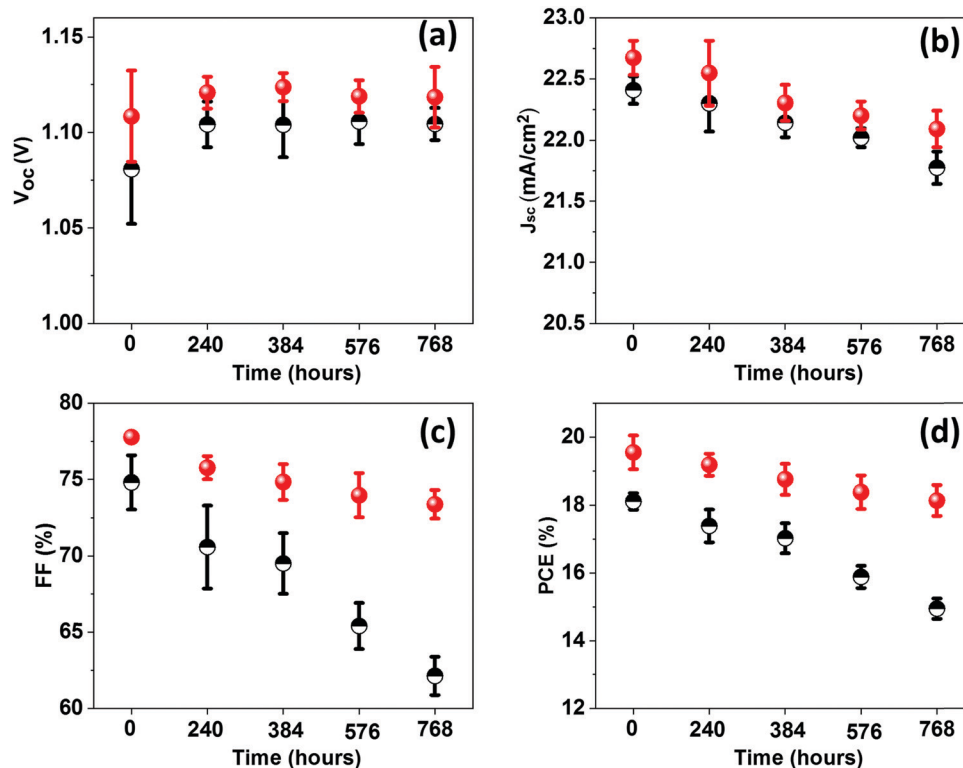
This journal is © The Royal Society of Chemistry 2022

**Fig. 5** The photovoltaic parameters ($V_{oc}$, $J_{sc}$, FF and PCE) of the pristine (black colour) and 5 mg mL$^{-1}$ CBSC passivated perovskite solar cells (red colour) for the duration of 768 hours in the dried box.

for each concentration and the performance is presented in the statistical distribution shown in Fig. 4f–i. It is obvious that the passivation with CBSC, regardless of concentration employed, achieved superior efficiency attributed to the heightened $V_{oc}$ and FF. The average PCEs of the 0 mg mL$^{-1}$ (pristine), 2 mg mL$^{-1}$, 5 mg mL$^{-1}$, and 7 mg mL$^{-1}$ CBSC based devices are 17.65%, 18.88%, 19.38% and 18.65%, respectively. Long-term stabilities of the pristine and CBSC passivated devices were tested under 30% relative humidity and room temperature for 768 hours, as shown in Fig. S6 and Table S3 (ESI†). The pristine device shows a large drop in PCE (from 18.29% to 15.09%), while the CBSC-passivated device exhibits a slight decrease in PCE from 20.02% to 18.66%. Fig. 5(a–d) present the long–term stability of the devices categorized according to the different photovoltaic parameters. The pristine device retains 82% of its initial PCE after 768 hours, while the CBSC-passivated device maintains 93% of its initial PCE under the same conditions.

## 3. Conclusion

In summary, deposition of the CBSC film at the perovskite/spiro-OMeTAD interface demonstrated effective passivation, which reduces surface defects. When the optimal concentration of CBSC was employed, a nonpareil PCE, reproducibility, and device stability were attained. The 5 mg mL$^{-1}$ CBSC passivated perovskite device achieved a maximum PCE of 20.02%, attributed to the improved FF and $V_{oc}$ attained. Excellent long-term

stability was also exhibited, retaining 93% of its initial PCE after 768 hours in the absence of encapsulation.

## 4. Experimental section

### Device fabrication

The fluorine–doped tin oxide (FTO) glass substrates were cleaned (detergent, deionized water, acetone, ethanol, and 2-propanol) and treated with ultraviolet ozone (20 min). The compact-TiO$_2$ film was deposited on the FTO substrates at 3000 rpm for 40 s and annealed at 500 °C for 1 h. Then, a SnO$_2$ layer was spin-coated on the TiO$_2$ surface at 5000 rpm for 20 sec and heated at 200 °C for 1 h. The triple cation perovskite precursor solution was prepared by dissolving MABr (28 mg), PbBr$_2$ (101) mg, FAI (215 mg), PbI$_2$ (633.8 mg), and 52.6 μL (39 mg of CsI in 100 μL of DMSO) in 1 mL of a mixture of DMF and DMSO (4 : 1 volume ratio). The perovskite precursor (40 μL) solution was deposited on TiO$_2$/SnO$_2$ substrates at 1000 rpm for 10 s and 6000 rpm for 25 s and 100 μL chlorobenzene was added dropwise in the last 10 s and heated at 100 °C for 1 h. For 4-chlorobenzene sulfonyl chloride (CBSC, ClC$_6$H$_4$SO$_2$Cl) passivation, various concentrations of CBSC (3, 5, and 7 mg mL$^{-1}$ in chlorobenzene) were deposited on the perovskite films and then heated at 100 °C for 10 min. The hole transport layer was deposited on the perovskite film at 4000 rpm for 30 sec using 1 mL chlorobenzene, Spiro-OMeTAD (70 mg mL$^{-1}$), 4-tert-butylpyridine (28 μL), bis(trifluoro-methylsulfonyl)amine lithium salt (16.94 μL; 520 mg mL$^{-1}$ in acetonitrile) and FK209 Co(III) TFSI Salt (35 μL; 37.6 mg/100 μL in

This journal is © The Royal Society of Chemistry 2022

J. Mater. Chem. C, 2022, **10**, 9044–9051 | **9049**

acetonitrile). Finally, an 80 nm gold electrode was deposited by thermal evaporation under a high vacuum.

### Characterization

The X-ray diffraction (XRD) measurements were measured with a Bruker D8 Advance diffractometer. The field emission scanning electron microscope (FESEM) characterization was performed by a JEOL JSM-7600F. X-ray photoelectron spectroscopy (XPS) was performed by a Kratos - AXIS Supra photoelectron spectrometer. The UV-Vis absorption spectra were recorded by a UV-1800 Shimadzu Spectrophotometer. The photoluminescence (PL) measurements were performed by RF-5301PC Shimadzu spectrophotometer. TRPL decay spectra were measured using a time-correlated single photon counting system (PicoQuant, PicoHarp 300). ATR-FTIR measurements were performed by using a Frontier Perkin Elmer instrument. The dark $I$–$V$ characteristics of electron only devices were measured using a Keithley 2400 source meter. The current density- voltage ($J$–$V$) characteristics of the devices were determined by a Keithley 2612A source meter with a scan rate of 300 mV s$^{-1}$. The incident photon-to-current efficiency (IPCE) spectra were tested on a PVE300 (Bentham) measurement system.

## Conflicts of interest

There are no conflicts to declare.

## Acknowledgements

## References

1 M. Shao, T. Bie, L. Yang, Y. Gao, X. Jin, F. He, N. Zheng, Y. Yu and X. Zhang, *Adv. Mater.*, 2021, **34**, 2107211.

2 Q. Zhou, Y. Gao, C. Cai, Z. Zhang, J. Xu, Z. Yuan and P. Gao, *Angew. Chem.*, 2021, **133**, 8384.

3 B. Wang, H. Li, Q. Dai, M. Zhang, Z. Zou, J. Brédas and Z. Lin, *Angew. Chem.*, 2021, **133**, 17805.

4 C. Y. Chang and C. C. Wang, *J. Mater. Chem. A*, 2020, **8**, 8593.

5 D. G. Lee, D. H. Kim, J. M. Lee, B. J. Kim, J. Y. Kim, S. S. Shin and H. S. Jung, *Adv. Funct. Mater.*, 2021, **31**, 2006718.

6 J. J. Yoo, G. Seo, M. R. Chua, T. G. Park, Y. Lu, F. Rotermund, Y. K. Kim, C. S. Moon, N. J. Jeon, J. P. Correa-Baena, V. Bulović, S. S. Shin, M. G. Bawendi and J. Seo, *Nature*, 2021, **590**, 587.

7 W. E.-I. Sha, X. Ren, L. Chen and W. C.-H. Choy, *Appl. Phys. Lett.*, 2015, **106**, 221104.

8 C. Ma and N. G. Park, *Chem*, 2020, **6**, 1254.

9 C. M. Wolff, P. Caprioglio, M. Stolterfoht and D. Neher, *Adv. Mater.*, 2019, **31**, 1902762.

10 M. Stolterfoht, P. Caprioglio, C. M. Wolff, J. A. Márquez, J. Nordmann, S. Zhang, D. Rothhardt, U. Hörmann, Y. Amir, A. Redinger, L. Kegelmann, F. Zu, S. Albrecht, N. Koch, T. Kirchartz, M. Saliba, T. Unold and D. Neher, *Energy Environ. Sci.*, 2019, **12**, 2778.

11 Y. Pei, Y. Liu, F. Li, S. Bai, X. Jian and M. Liu, *iScience*, 2019, **15**, 165.

12 W. Shen, Y. Dong, F. Huang, Y.-B. Cheng and J. Zhong, *Mater. Rep. Energy*, 2021, **1**, 100060.

13 J. Ye, M. M. Byranvand, C. O. Martínez, R. L.-Z. Hoye, M. Saliba and L. Polavarapu, *Angew. Chem., Int. Ed.*, 2021, **60**, 21636.

14 W. Kong, T. Ding, G. Bi and H. Wu, *Phys. Chem. Chem. Phys.*, 2016, **18**, 12626.

15 A. R. Bin Mohd Yusoff, M. Vasilopoulou, D. G. Georgiadou, L. C. Palilis, A. Abate and M. K. Nazeeruddin, *Energy Environ. Sci.*, 2021, **14**, 2906.

16 M. Yang, T. Tian, W. Feng, L. Wang and W.-Q. Wu, *Accounts Mater. Res.*, 2021, **2**, 1141.

17 S. Rahmany and L. Etgar, *Mater. Adv.*, 2021, **2**, 2617.

18 Z. Zhang, Y. Gao, Z. Li, L. Qiao, Q. Xiong, L. Deng, Z. Zhang, R. Long, Q. Zhou, Y. Du, Z. Lan, Y. Zhao, C. Li, K. Müllen and P. Gao, *Adv. Mater.*, 2021, **33**, 2008405.

19 X. Li, W. Sheng, X. Duan, Z. Lin, J. Yang, L. Tan and Y. Chen, *ACS Appl. Mater. Interfaces*, 2021, DOI: 10.1021/acsami.1c08539.

20 W. Zhang, Q. S. Li and Z. S. Li, *Appl. Surf. Sci.*, 2021, **563**, 150267.

21 C. C. Chueh, C. Z. Li and A. K.-Y. Jen, *Energy Environ. Sci.*, 2015, **8**, 1160.

22 E. Ochoa-Martinez, M. Ochoa, R. D. Ortuso, P. Ferdowsi, R. Carron, A. N. Tiwari, U. Steiner and M. Saliba, *ACS Energy Lett.*, 2021, **6**, 2626.

23 Q. Jiang, Y. Zhao, X. Zhang, X. Yang, Y. Chen, Z. Chu, Q. Ye, X. Li, Z. Yin and J. You, *Nat. Photonics*, 2019, **13**, 460.

24 J. Peng, Y. Wu, W. Ye, D. A. Jacobs, H. Shen, X. Fu, Y. Wan, T. Duong, N. Wu, C. Barugkin, H. T. Nguyen, D. Zhong, J. Li, T. Lu, Y. Liu, M. N. Lockrey, K. J. Weber, K. R. Catchpole and T. P. White, *Energy Environ. Sci.*, 2017, **10**, 1792.

25 D. H. Kang, S. Y. Kim, J. W. Lee and N. G. Park, *J. Mater. Chem. A*, 2021, **9**, 3441.

26 E. A. Alharbi, A. Y. Alyamani, D. J. Kubicki, A. R. Uhl, B. J. Walder, A. Q. Alanazi, J. Luo, A. Burgos-Caminal, A. Albadri, H. Albrithen, M. H. Alotaibi, J. E. Moser, S. M. Zakeeruddin, F. Giordano, L. Emsley and M. Grätzel, *Nat. Commun.*, 2019, **10**, 3008.

27 Z. Liu, F. Cao, M. Wang, M. Wang and L. Li, *Angew. Chem., Int. Ed.*, 2020, **59**, 4161.

28 X. Yi, Y. Mao, L. Zhang, J. Zhuang, Y. Zhang, N. Chen, T. Lin, Y. Wei, F. Wang, J. Wang and C. Li, Small, *Methods*, 2021, **5**, 2000441.

29 L. Huang, G. Wang, W. Zhou, B. Fu, X. Cheng, L. Zhang, Z. Yuan, S. Xiong, L. Zhang, Y. Xie, A. Zhang, Y. Zhang, W. Ma, W. Li, Y. Zhou, E. Reichmanis and Y. Chen, *ACS Nano*, 2018, **12**, 4440.

**9050** | *J. Mater. Chem. C*, 2022, **10**, 9044–9051

This journal is © The Royal Society of Chemistry 2022

30  B. Roose, K. Dey, Y. H. Chiang, R. H. Friend and S. D. Stranks, *J. Phys. Chem. Lett.*, 2020, **11**, 6505.

31  B. Wook Park, N. Kedem, M. Kulbak, D. Y. Lee, W. S. Yang, N. J. Jeon, J. Seo, G. Kim, K. J. Kim, T. J. Shin, G. Hodes, D. Cahen and S. Il Seok, *Nat. Commun.*, 2018, **9**, 93301.

32  T. Meier, T. P. Gujar, A. Schönleber, S. Olthof, K. Meerholz, S. Van Smaalen, F. Panzer, M. Thelakkat and A. Köhler, *J. Mater. Chem. C*, 2018, **6**, 7512.

33  F. Liu, Q. Dong, M. K. Wong, A. B. Djurišić, A. Ng, Z. Ren, Q. Shen, C. Surya, W. K. Chan, J. Wang, A. M.-C. Ng, C. Liao, H. Li, K. Shih, C. Wei, H. Su and J. Dai, *Adv. Energy Mater.*, 2016, **6**, 1502206.

34  X. Wang, Y. Qiu, L. Wang, T. Zhang, L. Zhu, T. Shan, Y. Wang, J. Jiang, L. Kong, H. Zhong, H. Yu, F. Liu, F. Gao, F. Wang and C. C. Chen, *Nano Energy*, 2021, **89**, 106445.

35  F. Zhang, J. Song, R. Hu, Y. Xiang, J. He, Y. Hao, J. Lian, B. Zhang, P. Zeng and J. Qu, *Small*, 2018, **14**, 1704007.

36  T. S. Sherkar, C. Momblona, L. Gil-Escrig, J. Ávila, M. Sessolo, H. J. Bolink and L. J.-A. Koster, *ACS Energy Lett.*, 2017, **2**, 1214.

37  H. Pan, H. Shao, X. L. Zhang, Y. Shen and M. Wang, *J. Appl. Phys.*, 2021, **129**, 130904.

38  R. Zheng, S. Zhao, H. Zhang, H. Li, J. Zhuang, X. Liu, H. Li and H. Wang, *Sol. Energy*, 2021, **224**, 472.

39  A. Kanwat, B. Ghosh, S. E. Ng, P. J.-S. Rana, Y. Lekina, T. J.-N. Hooper, N. Yantara, M. Kovalev, B. Chaudhary, P. Kajal, B. Febriansyah, Q. Y. Tan, M. Klein, Z. X. Shen, J. W. Ager, S. G. Mhaisalkar and N. Mathews, *ACS Nano*, 2022, **16**, 2942.

40  M. Vásquez-Montoya, J. F. Montoya, D. Ramirez and F. Jaramillo, *J. Energy Chem.*, 2021, **57**, 386.

41  X. Cheng, L. Huang, L. Zhang, Q. Ai, L. Chen and Y. Chen, *ACS Appl. Mater. Interfaces*, 2017, **9**, 9204.

42  X. Liu, Z. Yu, T. Wang, K. L. Chiu, F. Lin, H. Gong, L. Ding and Y. Cheng, *Adv. Energy Mater.*, 2020, **10**, 2001958.

43  B. Chen, P. N. Rudd, S. Yang, Y. Yuan and J. Huang, *Chem. Soc. Rev.*, 2019, **48**, 3842.

44  X. Zheng, B. Chen, J. Dai, Y. Fang, Y. Bai, Y. Lin, H. Wei, X. C. Zeng and J. Huang, *Nat. Energy*, 2017, **2**, 17102.

45  J. Hieulle, X. Wang, C. Stecker, D. Y. Son, L. Qiu, R. Ohmann, L. K. Ono, A. Mugarza, Y. Yan and Y. Qi, *J. Am. Chem. Soc.*, 2019, **141**, 3515.

46  G. Sadoughi, D. E. Starr, E. Handick, S. D. Stranks, M. Gorgoi, R. G. Wilks, M. Bär and H. J. Snaith, *ACS Appl. Mater. Interfaces*, 2015, **7**, 13440.

47  M. Thambidurai, B. Febriansyah, S. Foo, P. C. Harikesh, K. T. Ming, N. Mathews and C. Dang, *J. Power Sources*, 2020, **479**, 228811.

48  X. Gong, L. Guan, H. Pan, Q. Sun, X. Zhao, H. Li, H. Pan, Y. Shen, Y. Shao, L. Sun, Z. Cui, L. Ding and M. Wang, *Adv. Funct. Mater.*, 2018, **28**, 1804286.

49  S. Gharibzadeh, P. Fassl, I. M. Hossain, P. Rohrbeck, M. Frericks, M. Schmidt, T. Duong, M. R. Khan, T. Abzieher, B. A. Nejand, F. Schackmar, O. Almora, T. Feeney, R. Singh, D. Fuchs, U. Lemmer, J. P. Hofmann, S. A.-L. Weber and U. W. Paetzold, *Energy Environ. Sci.*, 2021, **14**, 5875.

50  S. Li, Z. He, Y. Li, K. Liu, M. Chen, Y. Yang and X. Li, *J. Alloys Compd.*, 2022, **889**, 161561.

51  W. Tress, N. Marinova, T. Moehl, S. M. Zakeeruddin, M. K. Nazeeruddin and M. Grätzel, *Energy Environ. Sci.*, 2015, **8**, 995.

This journal is © The Royal Society of Chemistry 2022

*J. Mater. Chem. C*, 2022, **10**, 9044–9051  |  **9051**